RSC Advances

ROYAL SOCIETY OF CHEMISTRY

www.rsc.org/advances

Journal Name

RSCPublishing

ARTICLE

Assembly of BF_4^-, PF_6^-, ClO_4^- and F^- with trinuclear copper(I) acetylide complexes bearing amide groups: Structural diversity, photophysics and anion binding properties

Cite this: DOI: 10.1039/xoxxoooooox

Received ooth January 2012,
Accepted ooth January 2012

DOI: 10.1039/xoxxoooooox

www.rsc.org/

Hua-Yun Shi, Yong-Liang Huang, Jia-Kai Sun, Ji-Jun Jiang, Zhi-Xing Luo, Hui-Tao Ling, Chi-Keung Lam and Hsiu-Yi Chao*

Trinuclear copper(I) acetylide complexes **1·BF4**–**4·BF4**, **1·PF6**, **1·ClO4** and **4·F** have been synthesized and characterized. Five kinds of discrete or polymeric structures could be found in their crystal structures. Among them, complexes **1·BF4**, **1·PF6**, and **1·ClO4** form zigzag one-dimensional (1D) anion coordination polymers (ACPs) using anions as nodes and cations **1** as ligands. For complex **2·BF4**, hydrogen bonds between adjacent amide groups afford the zigzag 1D polymeric chains, which are supported by the interaction between dppms and anions. A 1D infinite *meso*-helical hydrogen bonding polymeric chain with a counter anion bound in each cation can be observed in complex **3·BF4**. Complex **4·BF4** is unable to form polymeric chains, while complex **4·F** that exhibits similar structure with **4·BF4** could construct infinite 1D polymer *via* hydrogen bonds between amide groups. The photophysical properties of copper(I) acetylide complexes have been studied. They show luminescence both in the solid state and DMSO solution at 298 K. The anion binding abilities of complexes **1·BF4**–**4·BF4** in DMSO have also been studied by using ^{1}H NMR and UV-vis titration experiments. Their dramatic color change towards F^- in DMSO enables the naked eye detection of F^-.

Introduction

Anion coordination chemistry has attracted growing interest and developed rapidly in recent years, owing to the chemical, biological and environmental importance of anions.[1–8] In 1968, Park and Simmons[9] reported the first hydrogen bonding based halide sensor, which was regarded as the herald of the anion coordination chemistry. The concept of anion coordination was firstly proposed by Lehn[10] in 1978, which exhibited remarkable similarities and differences with traditional metal coordination chemistry. Compared with metal coordination, anion coordination is formed *via* the weak interactions (mainly hydrogen bond) between anions and ligands, rather than the covalent bond between ligands and metals. Owing to the diverse range of sizes, geometries, basicities and hydrogen-bonding modes of different anions, complexation of anions with the receptor molecules is highly challenging and requires delicate designs of host molecules.[11] The groups of Beer,[12–15] Gale,[16–19] Steed,[20–23] Custelcean,[24–27] Wu[28–32] and others[33–36] have reported novel anion-based architectures and studied their anion-binding modes, anion separation properties and fluorescence properties. Notably, supramolecular architectures with anions as the coordination nodes and organic ligand or metal complexes as linkers, bearing infinite polymeric nature, are defined as anion coordination polymer (ACPs) and yet to be explored[17, 18, 21, 27, 28, 37]. In contrast to the well-developed metal coordination polymers (CPs), in which metals with specific geometrical preference are employed as nodes, the construction of ACPs is imposed with more difficulties due to the weaker bonding strength of hydrogen bond and higher complexity of anions.[11] ACPs not only have potential applications as sensors[28, 37] or optical materials,[32, 37] but also exhibit structural and topological novelty with diverse and interesting structural motifs. The simplest type of ACPs, 1D-ACPs, which usually bear properties[38–39] such as anion exchange, gelation, and nanocrystal synthetic template, exhibit diverse polymeric architectures[38] such as linear, zigzag, helical, and ladder. The key factors that could affect the structures of ACPs are the building blocks: metal, ligands, and counter anions.[28, 40] Previous works included sulfate directed double strand helical self-assembly of chiral bicyclic guanidinium tetramers firstly reported by Mendoza's group,[41] 1D linear ACPs with acetate or terephthalate carboxylate anions and a bis-bisurea ligand based on a biphenyl backbone published by Gale's group,[17] chloride bridged supramolecular polymeric network with BF_2 complexes of acyclic dipyrrolyldiketone constructed by Maeda's group,[37] and a series of ACPs with a bis-bisurea ligand that bears a rigid naphthylene spacer as a linker between two anions, including SO_4^{2-}, AcO^-, $[COO–C_6H_4–COO]_2^-$, Cl^-, and Br^-, studied by Wu's group.[28]

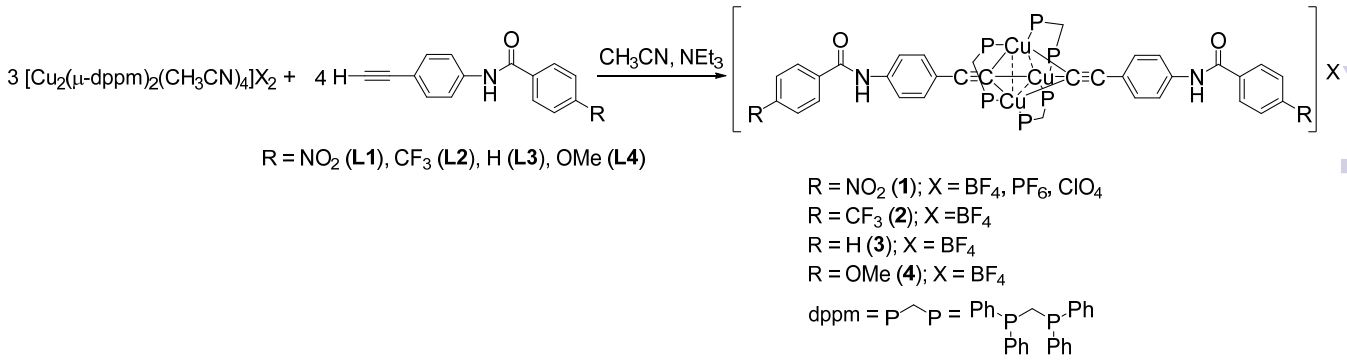

Scheme 1 Synthetic route for trinuclear copper(I) acetylide complexes **1·BF₄**–**4·BF₄**, **1·PF₆**, and **1·ClO₄**.

To date, however, anion-templated polymeric assemblies are very rare, and most of well-studied structures employed organic receptors as linkers.[40]

In the past decades, metal complexes have been frequently used as anion sensors due to their properties like redox and luminescence, which could provide various accesses of sensing.[42] Trinuclear copper(I) acetylide complexes have attracted considerable attention because of their rich photophysical and photochemical properties.[43–47] The first trinuclear copper(I) complex with two capped μ_3-η^1-acetylides with short Cu(I)···Cu(I) distances, [Cu₃(μ-dppm)₃(μ_3-η^1-C≡CPh)₂](BF₄) (dppm = bis(diphenylphosphino) methane), was reported by Gimeno and co-workers[48] in 1991. Subsequently, a systematical investigation on the photophysical properties of bicapped trinuclear copper(I) acetylide complexes was performed by Yam's group.[43–47] Our group[49] also reported a series of trinuclear copper(I) acetylide complexes bearing carbonyl moiety. However, research on trinuclear copper(I) acetylide complexes as anion sensors is still blank.

Neutral N–H or cationic $(N–H)^+$ hydrogen bond donor is a key component of anion receptors, and amide-based ligands belong to the neutral-type anion receptors.[50] It is interesting to note that anion binding by proteins is mostly achieved by way of neutral amide functional groups.[51] The highly accessible hydrogen-bond donor with directional hydrogen-bonding being involved for the host–guest interaction[11] provides amide receptors with a differentiating power to screen anions of different geometries or hydrogen bonding requirements.[52] These features, combined with their simple structures and easy modification by organic synthesis, make amide groups commonly be employed in the design of anion sensors. The supporting interactions between appropriately placed backbone C–H protons and anions are essential as well and enhance the anion-binding affinity.[22, 53–56] In some cases, C–H sites associate with anions without the supporting N–H. [53–56] Theoretical studies also support the interactions between C–H units and anions.[57–58] Aromatic C–Hs involve in the interaction with anions most frequently, while Maeda's group[37] reported the first example of anion recognition assisted by nonaromatic C–H···anion interactions.

Transition metal complexes with amide N–H hydrogen bond donor as anion-binding sites are our group's long-term interest.[59] Complexes with different R substituents exhibit varied affinities toward anions compared with their analogues,[59] we therefore envisaged that the acidity of amide groups could influence their coordination patterns and selective crystallization to anions. In this work, we have synthesized and characterized a series of trinuclear copper(I) acetylide complexes, [Cu₃(μ-dppm)₃(μ_3-η^1-C≡CC₆H₄-4-NHC(O)C₆H₄-4-R)₂]BF₄ (R = NO_2 (**1·BF₄**), H (**3·BF₄**) and OCH_3 (**4·BF₄**)), [Cu₃(μ-dppm)₃(μ_3-η^1-C≡CC₆H₄-4-NHC(O)C₆H₄-4-CF_3)(μ_2-η^1-C≡CC₆H₄-4-NHC(O)C₆H₄-4-CF_3)]BF₄ (**2·BF₄**), [Cu₃(μ-dppm)₃(μ_3-η^1-C≡CC₆H₄-4-NHC(O)C₆H₄-4-NO_2)₂]X (X = **PF₆** (**1·PF₆**) and ClO_4 (**1·ClO₄**)), and [Cu₃(μ-dppm)₃(μ_3-η^1-C≡CC₆H₄-4-NHC(O)C₆H₄-4-OCH_3)₂]F (**4·F**). The X-ray crystal structures of anion complexes **1·BF₄**–**4·BF₄**, **1·PF₆**, **1·ClO₄** and **4·F** were analyzed in detail to investigate the influence of anion as well as substitutents on polymeric architectural diversity. The photophysics of acetylide ligands and complexes as well as anion binding properties of complexes **1·BF₄**–**4·BF₄** in DMSO solution were also studied.

Results and discussion

Syntheses and characterization

The synthetic route of trinuclear copper(I) acetylide complexes **1·BF₄**–**4·BF₄**, **1·PF₆** and **1·ClO₄** is summarized in scheme 1. Acetylide ligands **L1**–**L4** were obtained by using similar methods reported in our previous paper.[59] The reactions of dinuclear complexes [Cu₂(μ-dppm)₂(CH_3CN)₄](X)₂ (X = BF_4^-, PF_6^-, or ClO_4^-) with **L1**–**L4** in the molar ration of 3:4 in degassed acetonitrile in the presence of triethylamine at 298 K gave trinuclear copper(I) acetylide complexes **1·BF₄**–**4·BF₄**, **1·PF₆** and **1·ClO₄**, respectively. All copper(I) acetylide complexes **1·BF₄**–**4·BF₄**, **1·PF₆** and **1·ClO₄** are air-stable in the solid state at 298 K and can be well dissolved in CH_2Cl_2, CH_3CN, THF and DMSO. They gave satisfactory elemental analysis and were all characterized by IR, ESI-MS and NMR.

The IR spectra of the trinuclear copper(I) acetylide complexes **1·BF₄**–**4·BF₄**, **1·PF₆**, and **1·ClO₄** contain three bands at *ca.* 3368–3399, 2170–2270 and *ca.* 1656–1677 cm^{-1}, which could be ascribed to ν(N–H), ν(C≡C) and ν(C=O) of acetylide ligands, respectively. In the ^{1}H NMR spectra, complexes **1·BF₄**–**4·BF₄**, **1·PF₆** and **1·ClO₄** in CD_3CN display a singlet at δ 8.90–9.30 ppm, which are assigned as the resonances of the amide N–H of the acetylide ligand. The chemical shifts of these peaks are in the following order: **1·BF₄** > **2·BF₄** > **3·BF₄** > **4·BF₄**, which is in line with the decreasing of the electron-withdrawing ability of substituent R (R = NO_2 (**1**), CF_3 (**2**), H (**3**), OCH_3 (**4**)) on the acetylide ligand. In addition, the chemical shifts at δ 6.64–8.54 ppm are attributed to the resonances of the protons on the aromatic rings of the dppm and acetylide ligands. A singlet at *ca.* δ 3.30 ppm is ascribed as the resonance of the protons of CH_2 moieties on dppm ligands. The ^{31}P NMR spectra of the complexes **1·BF₄**–**4·BF₄**, **1·PF₆** and **1·ClO₄** in CD_3CN show a singlet at *ca.* δ −6.00 ppm. While complex **1·PF₆** in CD_3CN shows an additional quintet at *ca.* δ −144.65 ppm, which can be ascribed to the counter anion PF_6^-. As for ^{19}F NMR spectra in CD_3CN, complexes **1·BF₄**–**4·BF₄** display two singlet at *ca.* δ −151.65 and −151.70 ppm with a proportion of 1:4 in peak area, which could be

ascribed to BF_4^- (the natural abundance of ^{10}B to ^{11}B is 1/4). Complex **1·PF₆** shows a doublet at δ –73.53 ppm with a coupling constant of 700 Hz, owing to $^{31}P - ^{19}F$ coupling. Complex **4·F** was obtained by addition of excess amount of F^- into **4·BF₄** in CH_3CN. The IR, ESI-MS, ^1H NMR and ^{31}P NMR spectra of **4·F** are similar to those of **4·BF₄**.

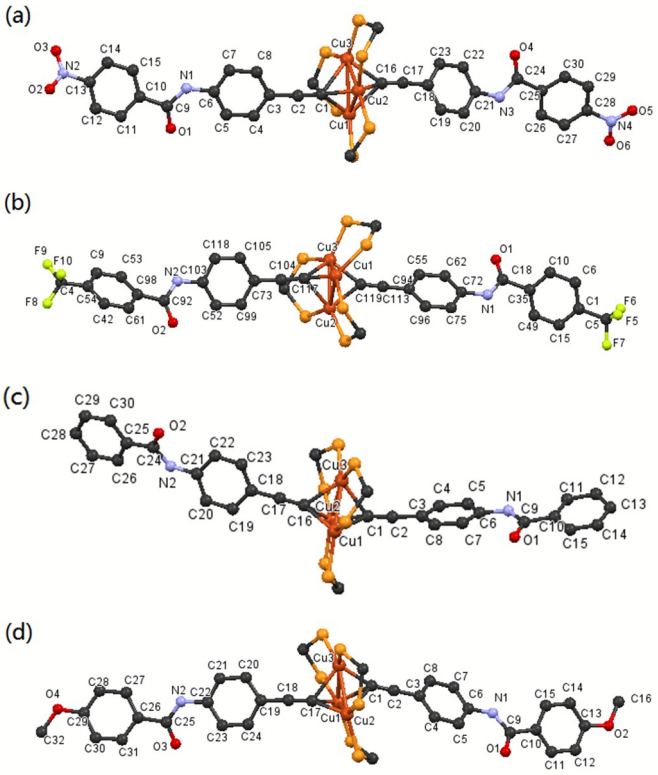

Fig. 1 The crystal structures of cations (a) **1**, (b) **2**, (c) **3**, and (d) **4** with the atomic numbering scheme (phenyl rings on dppm and hydrogen atoms are omitted for clarity). Thermal ellipsoids are shown at 30 % probability level.

X-ray crystal structure

Structures of cations 1–4

The crystals of complexes **1·BF₄**–**4·BF₄**, **1·PF₆**, **1·ClO₄** and **4·F** were obtained through the diffusion of ether into corresponding solution (**1·BF₄** and **2·BF₄** in CH_3CN, **1·PF₆** and **1·ClO₄** in CH_2Cl_2, **3·BF₄** and **4·F** in CH_3OH and **4·BF₄** in acetone and methanol mixed solution). Their crystallographic data as well as selected bond distances and angles are listed in Table S1–S6 (ESI†) and Table 1. The PXRD patterns (Fig. S1, ESI†) revealed the phase purity of complexes **1·BF₄**–**4·BF₄**, **1·PF₆**, **1·ClO₄** and **4·F** and indicated that the complexes were stable in air at room temperature. The perspective drawings of cations **1**–**4** are shown in Figure 1. Since the structures of cations **1**–**4** are similiar, **1·PF₆** is selected as an example for discussion. It crystallizes in the orthorhombic space group Pccn. The structure of the complex cation **1** is similar to those of previous reported $[Cu_3(\mu\text{-dppm})_3(\mu_3\text{-}\eta^1\text{-}C{\equiv}CR')_2]^+$ analogues,[43–49] which consists of an approximately isosceles triangle of copper atoms with a dppm ligand bridging each edge to form a roughly planar $[Cu_3P_6]$ core. The distances between two copper atoms are in the range of 2.5374(8)–2.7672(8) Å, which are shorter than the sum of van der Waals radii for copper atoms (2.8 Å).[60] This observation suggests the presence of weak Cu···Cu interactions. Three Cu_2P_2C rings adopt envelope conformations with the methylene carbon atoms on the flap. One of them folds toward one of the faces of the Cu_3 triangles, while the other two fold away from it. The Cu–P distances are in the range of 2.2549(12)–2.2948(11) Å, which resemble those in analogous trinuclear copper(I) acetylide complexes.[43–49] Two C≡C groups bridge the Cu_3 planar through an asymmetric μ_3-η^1 bridging mode with different Cu–C distances in the range of 2.077(4)–2.411(4) Å (for **2** exclusively, one of the C≡C group employs an asymmetric μ_2-η^1 bridging mode). It is noted that one of the three Cu–C distances is relatively longer than the other two Cu–C distances. The bond angles between the acetylide ligands and copper atoms in cation **1** are in the range of 123.0(4)°–159.1(4)°. The C≡C bond distances are 1.197(6) and 1.203(6) Å, respectively characteristic of typical metal acetylide σ bonding.[61] The conformations of two acetylide motifs attached on Cu_3 are not exactly identical to each other, which could be deduced from their different torsion angles. In the first acetylide motif, the torsion angles of C(5)–C(6)–N(1)–C(9) and C(15)–C(10)–C(9)–N(1) are 4.00° and 24.41°, respectively. In the other motif, the torsion angles of C(22)–C(21)–N(3)–C(24) and C(26)–C(25)–C(24)–N(3) are 16.37° and 30.22°, respectively. Dihedral angle between plane O(1)–C(9)–N(1) and plane O(4)–C(24)–N(3) is 27.48°, suggesting two amide moieties point to different direction. The C=O distances for **1** are 1.202(6) and 1.214(7) Å, which resemble typical carbonyl groups in analogues amide receptors.[50, 59]

Table 1 Selected bond lengths (Å) and angles (°) for **1·PF₆**.

Cu(1)···Cu(2)	2.5653(8)
Cu(1)···Cu(3)	2.7672(8)
Cu(2)···Cu(3)	2.5374(8)
Cu(1)–C(1)	2.175(4)
Cu(2)–C(1)	2.077(4)
Cu(3)–C(1)	2.411(4)
Cu(1)–C(16)	2.310(4)
Cu(2)–C(16)	2.114(4)
Cu(3)–C(16)	2.135(4)
Cu(1)–P(4)	2.2914(12)
Cu(1)–P(5)	2.2616(13)
Cu(2)–P(2)	2.2824(11)
Cu(2)–P(3)	2.2832(11)
Cu(3)–P(1)	2.2948(11)
Cu(3)–P(6)	2.2549(12)
C(1)–C(2)	1.197(6)
C(16)–C(17)	1.203(6)
C(9)–O(1)	1.214(7)
C(24)–O(4)	1.202(6)
N(2)–O(2)	1.218(7)
N(2)–O(3)	1.210(7)
N(4)–O(5)	1.221(7)
N(4)–O(6)	1.223(7)
Cu(1)–C(1)–C(2)	124.3(4)
Cu(2)–C(1)–C(2)	159.1(4)
Cu(3)–C(1)–C(2)	123.0(4)
Cu(1)–C(16)–C(17)	123.5(3)
Cu(2)–C(16)–C(17)	150.0(4)
Cu(3)–C(16)–C(17)	132.8(4)
Cu(1)–C(1)–Cu(2)	74.18(14)
Cu(1)–C(1)–Cu(3)	74.02(13)
Cu(2)–C(1)–Cu(3)	68.39(12)
Cu(1)–C(16)–Cu(2)	70.71(12)
Cu(1)–C(16)–Cu(3)	76.89(13)
Cu(2)–C(16)–Cu(3)	73.33(14)

Structures of anion complexes

(1) Complexes with NO_2 group

In complex **1·PF₆**, hydrogen bonds are formed between hexafluorophosphate (PF_6^-) and amide N–Hs as well as hexafluorophosphate anion and aromatic C–Hs in acetylide ligands (Fig. 2(b)). Hexafluorophosphate anion in **1·PF₆** is five-coordinated. Each hexafluorophosphate anion is surrounded by two amide clefts of two trinuclear copper(I) complexes and coordinated mainly by two hydrogen bonds from amide groups, which were supplemented by three additional C–H···F interactions. The hydrogen bond distances (N···F) and angles of N–H···F in **1·PF₆** are in the range of 3.1336–3.2179 Å and 142°–154°, respectively (Table 2). The supporting interactions C–H···F are weaker than N–H···F with longer bond distances (C···F, 3.3152–3.3478 Å) and similar C–H···F angles (146°–155°). The dihedral angle of adjacent Cu_3 plane (plane Cu(1)–Cu(2)–Cu(3) and plane Cu(1′)–Cu(2′)–Cu(3′)) is 51.16°. Two adjacent "Cu_3 cluster ligands" around hexafluorophosphate anion are in a bended arrangement, with an dihedral angle between plane N(1)–C(9)–O(1) and plane N(3′)–C(24′)–O(4′) being 25.20°. As a ditopic anion binding ligand, each cation **1** binds two PF_6^- simultaneously. Therefore, complex **1·PF₆** shows an infinite one-dimensional structure, which can be viewed as anion coordination polymers, or ACPs, in which the hexafluorophosphate anions function as the coordination nodes like the metal ions in CPs. In this polymeric structure, the anions are regularly arranged in an almost linear array, and a 1D infinite zigzag hydrogen bonding polymeric chain are formed by the bended cation **1** together with bridged PF_6^- (Fig. 2(a)). The fluorine atoms F(3) in PF_6^- which is used to bind with amide group are regularly arranged in an almost linear array, wherein the distance between two adjacent F atoms and the F(3)···F(3)···F(3) angle are 18.79 Å and 172.54°, respectively.

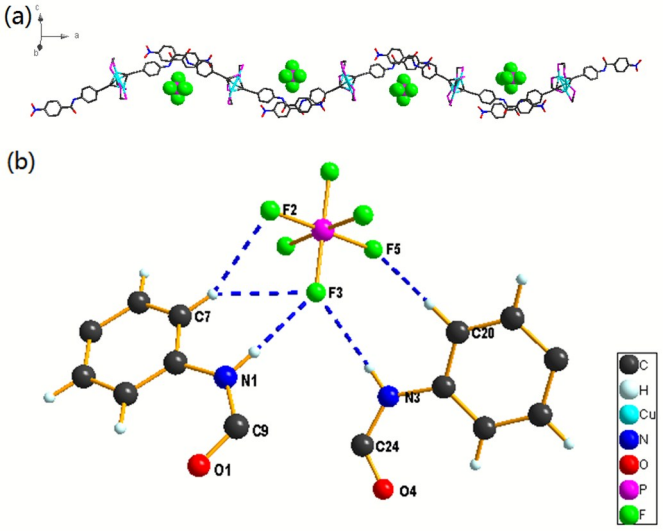

Fig. 2 The crystal structure of **1·PF₆**. (a) 1D ACPs; (b) anion coordination environment in ACPs.

Complexes **1·BF₄** and **1·ClO₄** adopt a similar structure with that of **1·PF₆** owing to the same substituent group NO_2 they have. The hydrogen bond distances and angles in **1·BF₄** and **1·ClO₄** are listed in Table 2. Each tetrafluoroborate or perchlorate anion is surrounded by two amide clefts of two trinuclear copper(I) complexes and coordinated mainly by two hydrogen bonds from amide groups, which were supplemented by additional C–H···F or C–H···O interactions (Fig. 3(b) and 4(b)). However, their configurations are affected by the counter anions with varied size, shape and basicity. In contrast to octahedral PF_6^-, BF_4^- and ClO_4^- with tetrahedral geometry in this system are three-coordinated. Only one atom in each anion is able to form hydrogen bond with two ligands in adjacent cations **1**. The hydrogen bond distances (N···F) and angles of N–H···F in **1·BF₄** are in the range of 2.9773–3.2826 Å and 138°–153°, respectively (Table 2). While the hydrogen bond distances (N···O) and angles of N–H···O in **1·ClO₄** are in the range of 3.075(9)–3.291(11) Å and 138°–155°, respectively (Table 2). The configuration of **1·BF₄** is supplemented by an additional C–H···F bond (C···F distance 3.3395 Å; C–H···F angle 152°), and **1·ClO₄** by a C–H···O bond (C···O distance 3.342(12) Å; C–H···O angle 152°). The stronger basicity of BF_4^- results in the shorter hydrogen bond distances in **1·BF₄** when compared with their counterparts in **1·ClO₄**. The dihedral angle of adjacent Cu_3 plane (plane Cu(1)–Cu(2)–Cu(3) and plane Cu(1′)–Cu(2′)–Cu(3′)) is 46.89° for **1·BF₄**, and 47.59° for **1·ClO₄**. Similar to the two unparalleled ligands in **1·PF₆**, the dihedral angle of plane N(120)–C(107)–O(117) and plane N(122′)–C(91′)–O(114′) is 26.02° in **1·BF₄**, and that of plane N(1)–C(9)–O(1) and plane N(3′)–C(24′)–O(4′) is 26.73° in **1·ClO₄**. Thus, ACPs **1·BF₄** and **1·ClO₄** adopt a 1D infinite zigzag structure as that of **1·PF₆**, with tetrahedral BF_4^- or ClO_4^- as node and bended cations **1** as ligand (Fig. 3(a) and 4(a)). The binding atoms F(1) in ACP **1·BF₄** and O(7) in ACP **1·ClO₄** are almost aligned (F(1)···F(1)···F(1) angle 175.32° and O(7)···O(7)···O(7) angle 176.03°), with the distances between two binding atoms are 18.79 Å (**1·BF₄**) and 18.81 Å (**1·ClO₄**), respectively.

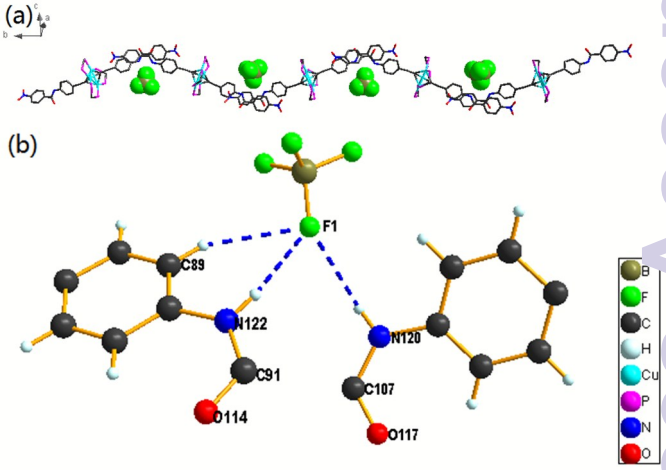

Fig. 3 The crystal structure of **1·BF₄**. (a) 1D ACPs; (b) anion coordination environment in ACPs.

(2) Complexes with CF_3 group

Infinite arrangement can also be found in complex **2·BF₄**, while in a different way from complexes with nitro group, owing to the differences in their shapes as well as electron-withdrawing properties. In **2·BF₄**, hydrogen bonds are formed between two adjacent amide N–Hs as well as tetrafluoroborate anions and aromatic C–Hs in dppm ligands (Fig. 5(b)). The hydrogen bond distances and angles in **2·BF₄** are listed in Table 2. Two amide groups in adjacent complex form the N–H···O hydrogen bond, which is the basic interaction in this system to maintain the polymeric structure. The two amide groups are in almost right-angle bended arrangement, with the dihedral angle of plane N(1)–C(18)–O(1) and plane N(2′)–C(92′)–O(2′) being 80.94°. The N–H···O hydrogen bonds with

N···O distance at 2.8566 Å and angle at 135°, respectively, are supplemented by two additional C–H···F interactions between dppm ligands and tetrafluoroborate anion. Tetrafluoroborate anions in **2·BF$_4$** are two-coordinated. The hydrogen bond distances (C···F) and angles of C–H···F in **2·BF$_4$** are in the range of 3.300(4)–3.459(5) Å and 139°–169°, respectively (Table 2). The dihedral angle of adjacent Cu$_3$ planes (plane Cu(1)–Cu(2)–Cu(3) and plane Cu(1′)–Cu(2′)–Cu(3′)) is 71.35°, which is in accord with the right-angle arrangement of amide groups. The dihedral angle between two benzene rings used to bind anions is 72.32°. In addition, the BF_4^- anions are regularly arranged in an almost right-angle array, wherein the distance between two boron atoms and the B(1)···B(1)···B(1) angle are 16.03 Å and 88.17°, respectively. Thus, complex **2·BF$_4$** can be regarded as a zigzag 1D ACP formed between cations **2** and bridged BF_4^- (Fig. 5(a)).

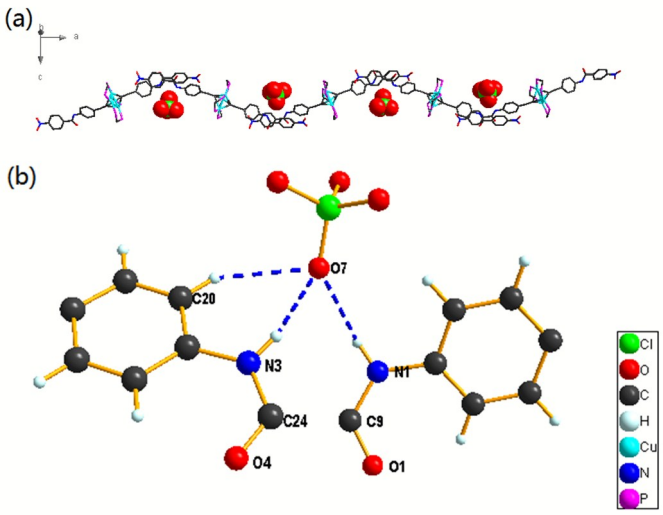

Fig. 4 The crystal structure of **1·ClO$_4$**. (a) 1D ACPs; (b) anion coordination environment in ACPs.

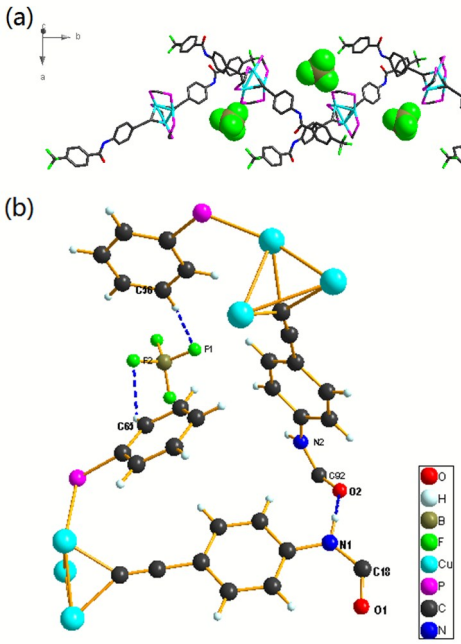

Fig. 5 The crystal structure of **2·BF$_4$**. (a) 1D ACPs; (b) anion coordination environment in ACPs.

(3) Complexes without substituent group

Different from complexes with electron-withdrawing groups, the cation **3** in complex **3·BF$_4$** could not bind two anions at the same time, and thus ACPs could not be observed in this system. In complex **3·BF$_4$**, anions BF_4^- are two-coordinated (Fig. 6(b)). A N–H···F hydrogen bond (N···F distance 2.870(6) Å; N–H···F angle 144°) and an additional C–H···F bond (C···F distance 3.381(7) Å, C–H···F angle 156°) are used to coordinate one of the amide groups in cation **3** (Table 2). In addition, two adjacent cations are interconnected *via* N(1)–H(1)···O(2) with N···O distance at 2.957(6) Å and angle at 154°, respectively, and two supporting interactions C(5)–H(5)···O(2) and C(11)–H(11)···O(2) (the C···O distances and angles range from 3.256(6)–3.333(9) Å and 144°–155°, respectively), which results in an infinite construction (Table 2). The dihedral angle of plane N(1)–C(9)–O(1) and plane N(2′)–C(24′)–O(2′) is 74.12° and the dihedral angle of adjacent Cu$_3$ planes (plane Cu(1)–Cu(2)–Cu(3) and plane Cu(1′)–Cu(2′)–Cu(3′)) is 86.63°, which is in accord with the right-angle arrangement of amide planes. As a ditopic ligand, cations **3** form a 1D infinite *meso* helical hydrogen bonding polymeric chain with a counter anion bound in each cation (Fig. 6(a)). The BF_4^- anions are regularly arranged in an almost right-angle array, wherein the distance between two boron atoms and the B(4)···B(4)···B(4) angle are 20.84 Å and 72.17°, respectively. The *meso*-helical chain in complex **3·BF$_4$** has a pitch length of 24.55 Å.

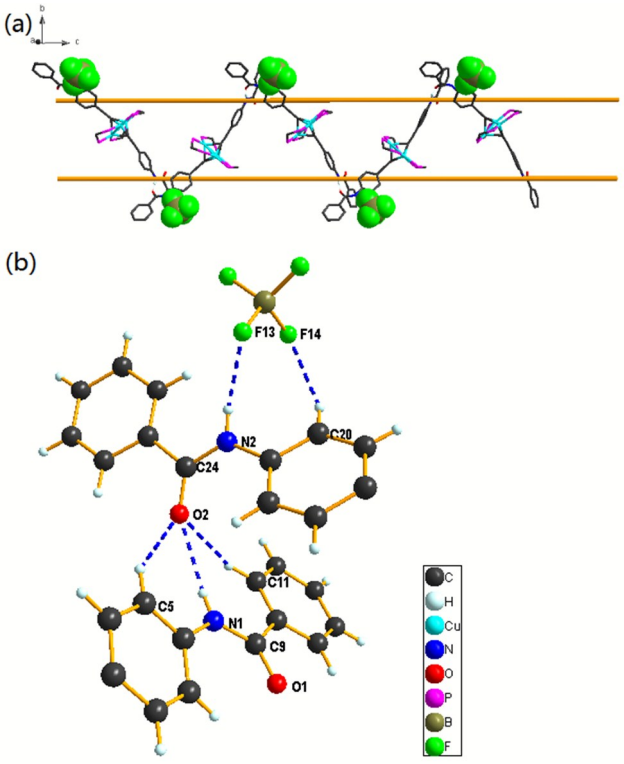

Fig. 6 The crystal structure of **3·BF$_4$**, (a) 1D polymeric chain; (b) anion coordination environment in ACPs.

(4) Complexes with OCH_3 group

In complex **4·BF$_4$**, one of the amide group in cation **4** coordinates the counter anion BF_4^- *via* a N–H···F hydrogen bond, which is supplemented by two additional C–H···F bonds (Fig.). Tetrafluoroborate anions in **4·BF$_4$** are three-coordinated. The

hydrogen bond distance and angle of N–H···F in **4·BF$_4$** are 3.077(6) Å and 162°, and those of C–H···F are in the range of 3.326(7)–3.343(8) Å and 144°–166°, respectively (Table 2). However, different from complexes with electron-withdrawing group, **4·BF$_4$** is unable to bind two anions simultaneously, therefore cannot construct stable polymeric chain using anions as nodes.

Complex **4·F** was obtained upon addition of excess fluoride anions into the solution of **4·BF$_4$**. Its structure is similar to complex **4·BF$_4$**, consisting of a bended cation **4** and a fluoride anion bound at one side by amide group (Fig. 8(b)). Hydrogen bonds involve fluoride anions in this system include N(1)–H(1A)···F(1) (N···F distance 2.805(3) Å; N–H···F angle 165°) and two additional C–H···F bonds (C···F distance 3.141(4)–3.189(4) Å; N–H···F angle 126°–140°) (Table 2). Due to the stronger basicity and smaller size of fluoride anion, the average hydrogen bond distance in **4·F** is shorter than **4·BF$_4$** considerably. Furthermore, resemble complex **3·BF$_4$**, two cations in **4·F** are held together by N(2)–H(2A)···O(1) (N···O distance 3.241(3) Å; N–H···O angle 146°), and supported by C(27)–H(27A)···O(1) (C···O distance 3.522(3) Å; C–H···O angle 168°). The dihedral angle of plane N(1)–C(9)–O(1) and plane N(2′)–C(25′)–O(3′) is 54.87°. Two adjacent Cu_3 planes (plane Cu(1)–Cu(2)–Cu(3) and plane Cu(1′)–Cu(2′)–Cu(3′)) are nearly parallel, with a dihedral angle being 0° and the identity distance being 15.94 Å. In the meanwhile, the anions are regularly arranged in an almost linear array, wherein the distance between two fluoride anions and the F(1)···F(1)···F(1) angle are 17.91 Å and 180.00°, respectively. Therefore, cations **4** together with F^- form the 1D infinite linear hydrogen bonding polymeric chains (Fig. 8(a)).

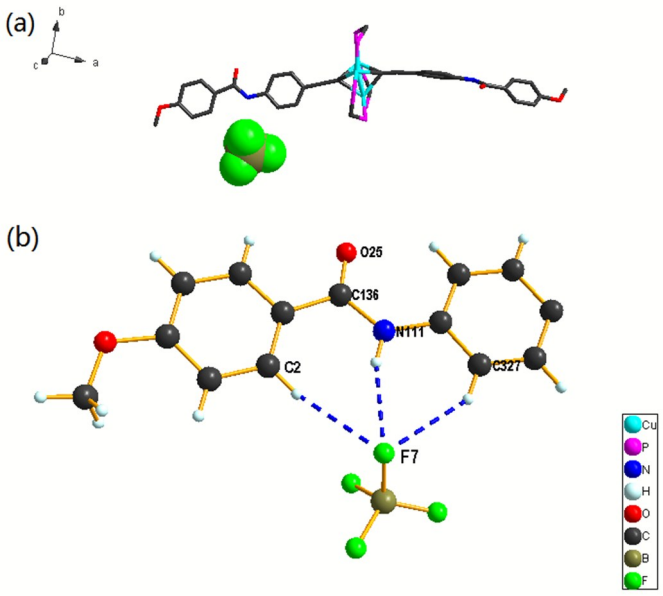

Fig. 7 (a) The crystal structure of **4·BF$_4$**; (b) anion coordination environment in **4·BF$_4$**.

(5) Structural diversity of complexes

Seven complexes reported in this work bear five kinds of architectures (Fig. 9). In complexes with nitro group **1·BF$_4$**, **1·PF$_6$**, and **1·ClO$_4$**, each anion is bound to two ligands from adjacent complexes at amide sites. In other words, 1D zigzag polymeric chains are formed using anions as node and complexes as cations. In this case, difference in anions results merely in different angles, rather than diverse architectures. When compared with nitro-substituted complexes, complexes with less electron-withdrawing group **2·BF$_4$** are unable to bind anions by their amide groups, due to the less acidity of amide N–Hs here. In **2·BF$_4$**, zigzag polymeric chains are formed *via* hydrogen bonds between two amide groups in adjacent complexes and supported by interactions between dppm ligands and tetrafluoroborate anion. While in complex without substituent group **3·BF$_4$**, 1D ACP could not be observed owing to the absence of the electron-withdrawing group. However, adjacent cations are interconnected to construct a 1D infinite *meso*-helical hydrogen bonding polymeric chain with a counter anion bound in each cation. As for complexes with electron-donating group, **4·BF$_4$** and **4·F**, structures varied dramatically with different anions. Owing to the weak hydrogen bond donor in **4·BF$_4$**, polymeric structure could not be found. However, with stronger base F^-, infinite linear chains are formed by amide groups' hydrogen bonds and anions are bound to one of the amide groups. As what we can see, assembly of various anions and cations with different substituent groups results in the diversity of trinuclear copper(I) acetylide complexes.

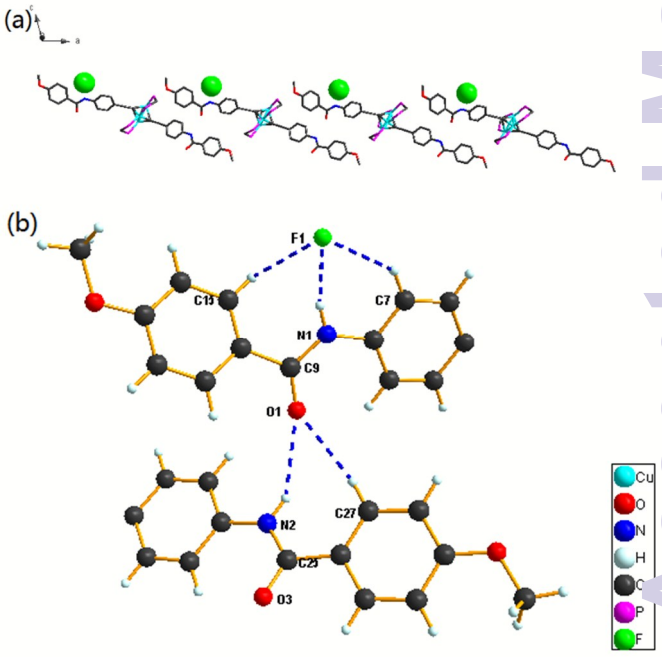

Fig. 8 The crystal structure of **4·F**, (a) 1D polymeric chain; (b) anion coordination environment in polymeric chain.

Electronic absorption and emission spectra of complexes 1·BF$_4$–4·BF$_4$

The photophysical data for complexes **1·BF$_4$**–**4·BF$_4$**, **1·PF$_6$**, **1·ClO$_4$** and **4·F** are summarized in Table 3. For comparison, the photopysics of acetylide ligands **L1**–**L4** are studied and listed in Table S7 (ESI†) as well. The electronic absorption spectrum of **1·BF$_4$** in DMSO at 298 K (Fig. S2, ESI†) shows a high-energy band at *ca*. 266 and a shoulder at *ca*. 302 nm, which are assigned to ligand-centred $\pi \rightarrow \pi^*$(dppm) and $\pi \rightarrow \pi^*$(acetylide) transitions, respectively, owing to the similar absorption energies with those of the free dppm ligand and acetylenes. The lower energy absorption shoulder at *ca*. 336 nm is probably the charge transfer transition from the amide to the NO$_2$ group in the acetylide ligand. The electronic absorption spectra of complexes **1·PF$_6$** and **1·ClO$_4$** are similar to that of **1·BF$_4$** (Fig. S2, ESI†), indicating that counter anions exert slight effect on absorption intensity and wavelength. The electronic absorption spectra of non-nitro derivatives **2·BF$_4$**–**4·BF$_4$** in DMSO at 298 K (Fig. S3, ESI†) exhibit two absorption bands at *ca*. 268 and 345–350 nm. The band

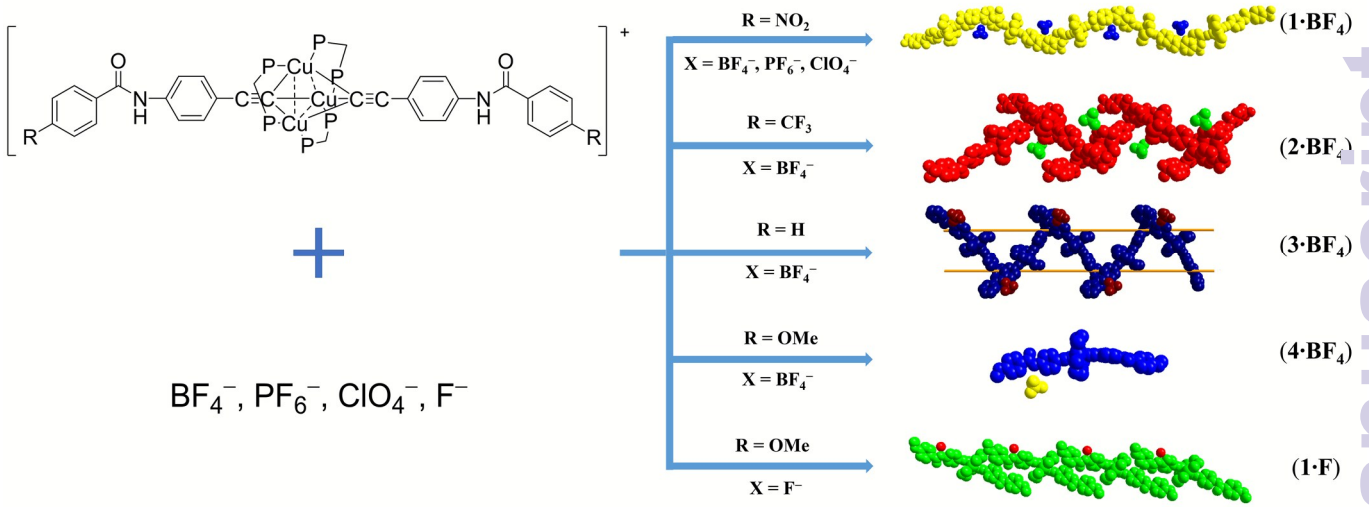

Fig. 9 Polymeric structural diversity of complexes reported in this paper (for complexes with nitro group, **1·BF4** is shown as an example).

Table 2 Selected hydrogen bonding parameters for **1·BF4**, **1·PF6**, **1·ClO4**, **2·BF4**, **3·BF4**, **4·BF4** and **4·F**.

Complexes	D–H···A	d(D–H)	d(H···A)	d(D···A)	∠(DHA)	Symmetry Code
1·BF4	N(120)–H(12B)···F(1)	0.86	2.28	2.9773	138	
	N(122)–H(12A)···F(1)	0.86	2.49	3.2826	153	1–x, 1/2+y, 1/2-z
	C(89)–H(89A)···F(1)	0.93	2.49	3.3395	152	
1·PF6	N(1)–H(1)···F(3)	0.86	2.42	3.2179	154	–x, 1/2+y, 1/2-z
	N(3)–H(3)···F(3)	0.86	2.41	3.1336	142	1/2-x, 1/2-y, z
	C(7)–H(7)···F(2)	0.93	2.48	3.3478	155	–x, 1/2+y, 1/2–z
	C(7)–H(7)···F(3)	0.93	2.50	3.3259	147	–x, 1/2+y, 1/2–z
	C(20)–H(20)···F(5)	0.93	2.50	3.3152	146	1/2-x, 1/2-y, z
1·ClO4	N(1)–H(1)···O(7)	0.88	2.36	3.075(9)	138	3/2-x, 1/2-y, z
	N(3)–H(3)···O(7)	0.88	2.47	3.291(11)	155	2–x, 1/2+y, 1/2–z
	C(20)–H(20)···O(7)	0.95	2.47	3.342(12)	152	2–x, 1/2+y, 1/2–z
2·BF4	N(1)–H(1)···O(2)	0.86	2.18	2.852(3)	135	1/2–x, -1/2+y, 1/2–z
	C(56)–H(56)···F(1)	0.93	2.54	3.459(5)	169	x, 1+y, z
	C(65)–H(65)···F(2)	0.93	2.54	3.300(4)	139	1/2-x, 1/2+y, 1/2–z
3·BF4	N(1)–H(1)···O(2)	0.86	2.16	2.957(6)	154	x,-y,1/2+z
	C(5)–H(5)···O(2)	0.93	2.48	3.256(6)	142	x,-y,1/2+z
	C(11)–H(11)···O(2)	0.93	2.47	3.333(9)	155	x,-y,1/2+z
	N(2)–H(2)···F(13)	0.86	2.13	2.870(6)	144	
	C(20)–H(20)···F(14)	0.93	2.51	3.381(7)	156	
4·BF4	N(2)–H(2)···F(2)	0.88	2.23	3.077(6)	162	x, 1/2–y, 1/2+z
	C(21)–H(21)···F(2)	0.95	2.51	3.326(7)	144	x, 1/2–y, 1/2+z
	C(27)–H(27)···F(2)	0.95	2.41	3.343(8)	166	x, 1/2–y, 1/2+z
4·F	N(2)–H(2A)···O(1)	0.88	2.48	3.244(4)	146	1+x, y, z
	C(27)–H(27A)···O(1)	0.95	2.59	3.527(4)	168	1+x, y, z
	N(1)–H(1A)···F(1)	0.88	1.95	2.811(5)	165	–1/2+x, 3/2–y, 1/2+z
	C(7)–H(7A)···F(1)	0.95	2.40	3.189(5)	140	–1/2+x, 3/2–y, 1/2+z
	C(15)–H(15A)···F(1)	0.95	2.48	3.140(5)	126	–1/2+x, 3/2–y, 1/2+z

at *ca*. 268 nm is ascribed to ligand-centred π→ π* (dppm) transition, while low-energy bands at 345–350 nm are assigned as the admixture of metal-perturbed ligand-centered π-π* (acetylide) and LMCT (acetylide → Cu_3) transition.[44–45] **4·F** shows similar electronic absorption spectrum with **4·BF4**, expect for the slight decrease in the molar absorption coefficient (Fig. S4, ESI†).

Excitation at λ > 370 nm of complexes **1·BF4**–**4·BF4**, **1·PF6**, **1·ClO4** and **4·F** in the solid state and in DMSO solution results in long-lived and intense luminescence in the visible light regime at 298 K, with emission quantum yields of 1.4 × 10^{-2}–8.6 × 10^{-2} in DMSO solutions. Fig. 10 displays the emission spectrum of **3·BF4** in the solid state at 298 K, in which a broad band at *ca*. 514 nm and a shoulder at *ca*. 557 nm are observed. The spacing of the adjacent band **3·BF4** is *ca*. 1500 cm^{-1}, which is typical of ground-state aromatic *v* (C···C) stretching frequency.[45] The solid state emission spectra of **1·BF4**, **2·BF4**, **4·BF4**, **1·PF6**, **1·ClO4** and **4·F** (Figs. S5–10, ESI†) are similar to that of **3·BF4** with lifetimes in microsecond range, which is suggestive of the involvement of a spin-forbidden transition. In general, the complexes with electron-rich acetylides emit at a lower energy. The electron-donating substituent R would

increase the energy of the π orbital of the acetylides and thus decrease the energy of the LMCT excited state. Therefore, the origin of the emission is proposed to involve substantial ^{3}LMCT [acetylide → Cu_3] character.[44–45] In DMSO solution, trinuclear copper(I) acetylide complexes **1·BF$_4$–4·BF$_4$**, **1·PF$_6$**, **1·ClO$_4$** and **4·F** exhibit blue-green to yellow-green emission at 298 K (Fig. S11–17, ESI†). A broad band at *ca*. 475–500 nm is observed, which follows the same trend with that in solid state. Thus, the emission in DMSO solution is ascribed to LMCT as well.[44–45] For the trinuclear copper(I) acetylide complexes studied in this paper, the emission energies depend mainly on the substituent R on the acetylide ligand, while the type of counter anions have little effect on the electronic absorption as well as emission spectra both in solid state and DMSO solution.

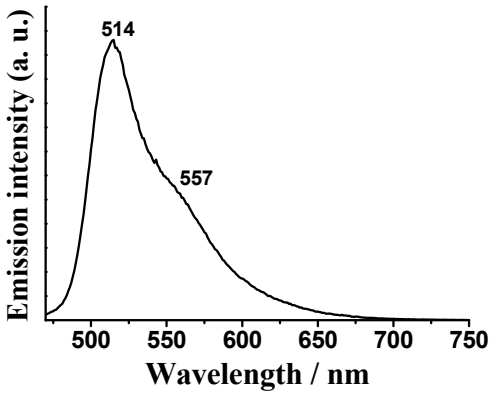

Fig. 10 Emission spectrum of **3·BF$_4$** in the solid state at 298 K (λ_{ex} = 428 nm).

Anion binding properties of complexes 1·BF$_4$–4·BF$_4$

The anion-binding properties of complexes **1·BF$_4$–4·BF$_4$** have been investigated by ^{1}H NMR spectroscopy. The results of ^{1}H NMR titration studies with a variety of anions show that even in a competitive solvent (DMSO–d_6) interactions and selectivity could still be observed. All of the anions used were in the form of tetra-*n*-butylammonium salts. Unfortunately, due to the decomposition of the trinuclear complexes upon addition of $NBu_4H_2PO_4$ and NBu_4HSO_4, the investigations toward $H_2PO_4^-$ and HSO_4^- were not carried out.

Fig. S18 (ESI†) shows the ^{1}H NMR spectral changes of **1·BF$_4$** upon addition of Cl^- in DMSO–d_6. Upon the addition of chloride anion, the signals of the N–H protons (H_a) show a relatively considerable downfield shift, while the other proton signals are found to undergo essentially negligible changes, which suggests the formation of a hydrogen bonding interaction between the amide groups in **1·BF$_4$** and Cl^-. The slight downfield shift of protons H_c and H_d on the phenyl ring is ascribed to the polarization effect of the C–H bond that is introduced by the through-space effect.[62–64] Analogous investigations have also been carried out with Y–shape anion OAc^- and larger halides Br^- and I^- (Fig. S19–21, ESI†). The magnitude of the complexation-induced ^{1}H NMR shift upon addition of OAc^- is larger when compared with that of Cl^-, while the signal of the N–H protons (H_a) shows slight change with Br^-, and none when I^- was added. For other complexes, **2·BF$_4$–4·BF$_4$**, the anion binding properties were also studied (Fig. 11 and S22, ESI†), which show similar binding trend with **1·BF$_4$**, but weaker binding ability.

Unfortunately, we were unable to obtain the anion-binding constants of complexes **1·BF$_4$–4·BF$_4$** by nonlinear least-square fits of the shifts of the signals of amide N–H (H_a) versus the concentration of the added anions, owing to the small changes in the amide N–H (H_a) chemical shifts. As a result, we could only compare the signal changes upon addition of different anions in the same amount. In general, the signal changes of different complexes with the same anion are in the following order: R = NO_2 (**1·BF$_4$**) > CF_3 (**2·BF$_4$**) > H (**3·BF$_4$**) > OCH_3 (**4·BF$_4$**), which is in line with the decreasing of the electron-withdrawing ability of substituent R on the acetylide ligands (Fig. S22, ESI†). This could be rationalized by the fact that the stronger electron-withdrawing substituent R on the acetylide ligand could induce higher acidity of amide group, which strengthen the hydrogen bond interactions between complexes and anions. The signal changes of the same complex with the various anions are in the following order: $OAc^- > Cl^- > Br^- > I^-$, which is in line with the decreasing of the basicity of anions (Fig. 11).

The interactions of **1·BF$_4$–4·BF$_4$** with F^- were investigated and exhibited different spectral changes from other anions. Fig. S23 (ESI†) shows the ^{1}H NMR spectral changes of **1·BF$_4$** in DMSO–d_6 upon addition of F^-. The significant downfield shift of the signal of amide N–H (H_a) is observed upon addition of F^- from 0 to 1 equiv, while this peak disappear rapidly when the amount of F^- added was larger than 1 equiv, and the aromatic proton signals H_b and H_d showed a slight upfield shift, which could be ascribed to the deshielding effect resulting from the increased electron density of the phenyl ring,[65] induced by the deprotonation of the amide N–H unit. During the addition of F^-, the color of the solution of **1·BF$_4$** in DMSO–d_6 changes from orange to dark red. After the addition of 3 equiv of F^-, a distinct triplet centered at 16.08 ppm (J = 120 Hz) appears, which is assigned as the formation of HF_2^-.[66–67] In addition, its ^{19}F NMR spectrum also displays a distinct doublet centered at −143.13 ppm (J = 117 Hz) (Fig. S24, ESI†), suggesting the formation of HF_2^-.[66–67] These results indicate the deprotonation of the amide N–H of **1·BF$_4$** upon addition of F^- in DMSO–d_6. Complexes **1·PF$_6$**, **1·ClO$_4$** and **2·BF$_4$–4·BF$_4$** show similar color and spectral changes upon addition of F^-, which could be ascribed to deprotonation as well (Fig. S25–S34, ESI†).

We have also examined the color change of complexes **1·BF$_4$** with different anions in DMSO (Fig. S35 and S36, ESI†). No color change of **1·BF$_4$** in DMSO could be observed upon addition of anions, except F^-. Thus, **1·BF$_4$** shows selective color change toward F^- in DMSO. Complexes **2·BF$_4$–4·BF$_4$** exhibited similar selectivity through dramatic color change, which allows F^- detection with naked eyes. Even though addition of the anions studied in this paper into the solutions of **1·BF$_4$–4·BF$_4$** did cause their UV-Vis spectral changes, the changes were too small to compare the binding abilities of complexes **1·BF$_4$–4·BF$_4$** towards anions.

Conclusions

In summary, a series of discrete or polymeric amide based trinuclear copper(I) complexes **1·BF$_4$–4·BF$_4$**, **1·PF$_6$**, **1·ClO$_4$** and **4·F** have been synthesized and characterized, with their crystal structures determined. Among them, 1 D hydrogen bonding polymeric chain with zigzag, *meso*-helical or linear structures are observed. The architectures of these complexes could be perturbed by anions and the R group on "Cu_3 cluster ligands". Complexes **1·BF$_4$–4·BF$_4$**, **1·PF$_6$**, **1·ClO$_4$** and **4·F** exhibit luminescence both in the solid state and in the DMSO solution at 298 K. The anion binding abilities of complexes **1·BF$_4$–4·BF$_4$** toward different anions have also been studied by NMR and UV-vis. Their selective color change upon addition of F^- enables the naked eye detection of F^-.

Table 3 Photophysical data of complexes **1·BF$_4$**–**4·BF$_4$**, **1·PF$_6$**, **1·ClO$_4$** and **4·F** at 298 K.

complexes	medium	λ_{abs} / nm (ε / dm^{3}mol^{-1}cm^{-1})	λ_{em} / nm (ε_{em} / τs)	Φ_{em}
1·BF$_4$	DMSO	266 (83540), 302 (sh, 60910), 336 (sh, 45460)	474 (0.1)	0.014
	solid		505 (7.3)	
1·PF$_6$	DMSO	266 (85860), 302 (sh, 63030), 336 (sh, 46570)	474 (0.1)	0.016
	solid		504 (max, 6.7), 544 (sh)	
1·ClO$_4$	DMSO	266 (90910), 302 (sh, 63430), 336 (sh, 44440)	474 (0.1)	0.015
	solid		506 (11.1)	
2·BF$_4$	DMSO	268 (58990), 350 (44950)	475 (0.1)	0.051
	solid		507 (14.7)	
3·BF$_4$	DMSO	268 (60810), 346 (45760)	502 (0.3)	0.078
	solid		514 (max, 75.3), 557 (sh)	
4·BF$_4$	DMSO	268 (58180), 345 (47880)	500 (0.3)	0.086
	solid		514 (max, 21.9), 557 (sh)	
4·F	DMSO	268 (55660), 345 (46970)	499 (0.3)	0.078
	solid		513 (25.1)	

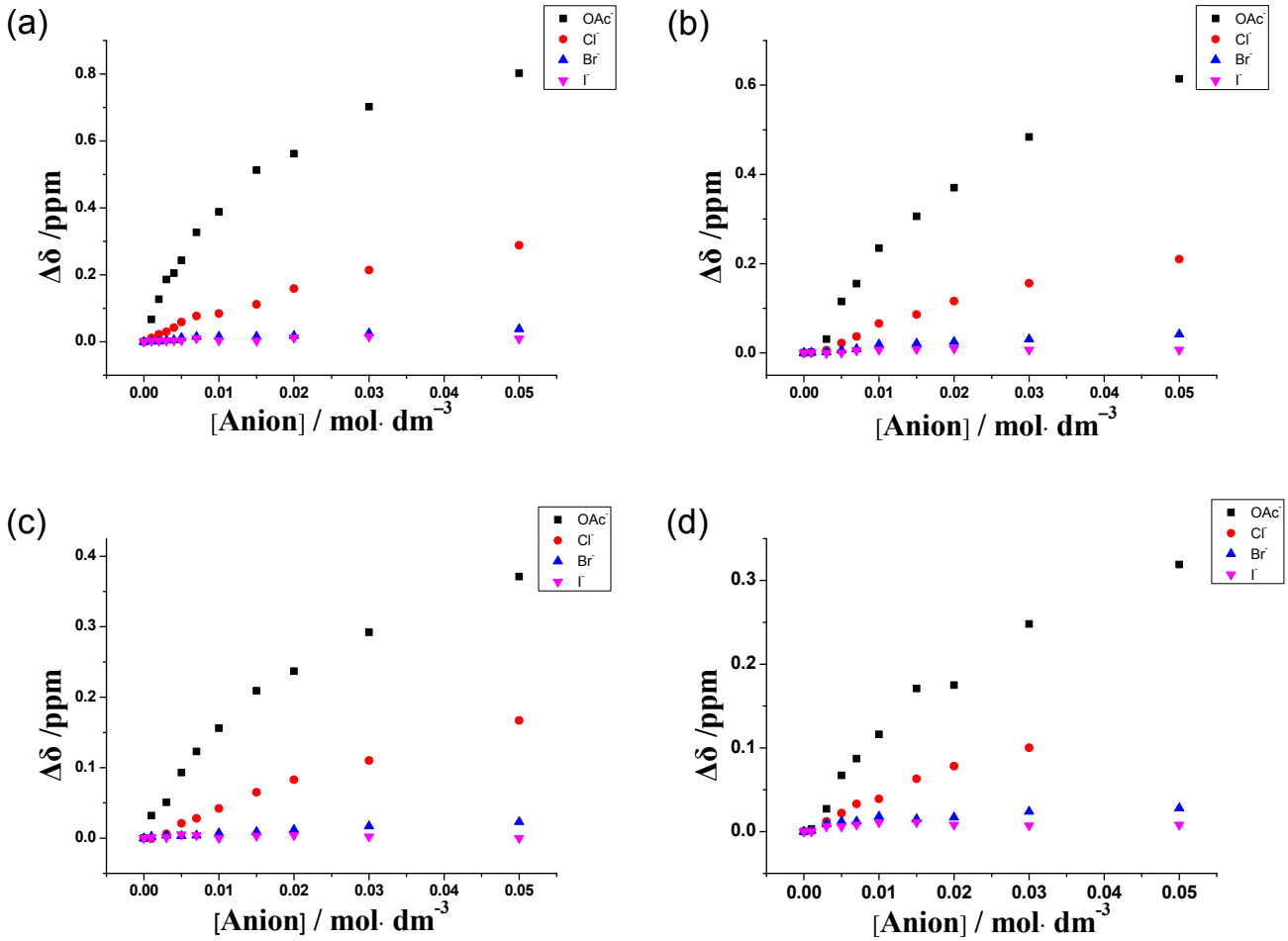

Fig. 11 The shifts of the signals of amide N–H (H$_a$) of complexes (a) **1·BF$_4$**, (b) **2·BF$_4$**, (c) **3·BF$_4$**, and (d) **4·BF$_4$** upon addition of different anions with different concentrations in DMSO–d_6 at 298 K.

Experimental section

Materials and reagents

Dinuclear complexes [Cu$_2$(μ-dppm)$_2$(CH$_3$CN)$_4$](BF$_4$)$_2$, [Cu$_2$(μ-dppm)$_2$(CH$_3$CN)$_4$](PF$_6$)$_2$, and [Cu$_2$(μ-dppm)$_2$(CH$_3$CN)$_4$](ClO$_4$)$_2$ were synthesized according to literature procedures.[68] Bis(diphenylphosphino)methane (dppm) and benzoyl chloride were purchased from Alfa–Aesar. 4–Ethylnylaniline and tetra-*n*-butylammonium iodide were purchased from Acros. 4–Nitrobenzoyl chloride was purchased from TCI. 4–Methoxybenzoyl, 4–trifluoromethylbenzoyl chloride and tetra–*n*–butylammonium bromide hydrate were obtained from J&K. Tetra–*n*–butylammonium fluoride hydrate and tetra–*n*–butylammonium acetate was obtained from Sigma–Aldrich. All reactions were carried out under anhydrous and anaerobic conditions using standard Schlenk techniques under

nitrogen. All solvents were purified and distilled using standard procedures before use. All other reagents were of analytical grade and were used as received.

Physical measurements and instrumentation

Chemical shifts (δ, ppm) were reported relative to tetramethylsilane for ^{1}H NMR, and NaF for ^{19}F NMR on a Varian Mercury–Plus 300 spectrometer, 85% H_3PO_4 for ^{31}P NMR on a Bruker Avance III 400 MHz spectrometer. Emission spectra were obtained on a FLS980 fluorescence spectrophotometer. The solution emission quantum yields were measured using quinine sulfate in 1.0 N sulfuric acid as standard[69] (Φ_r = 0.546, excitation wavelength at 365 nm) and calculated by $\Phi_{em} = \Phi_r (B_r/B_s)(n_s/n_r)^2(D_s/D_r)$, where the subscripts s and r refer to sample and reference standard solution respectively, n is the refractive index of the solvents, D is the integrated intensity, and Φ is the luminescence quantum yield. The quantity B is calculated by $B = 1–10^{-AL}$, where A is the absorbance at the excitation wavelength and L is the optical path length. Infra–red spectra were recorded from KBr pellets in the range of 400–4000 cm^{-1} on a Bruker–EQUINOX 55 FT–IR spectrometer. Electrospray ionization (ESI) mass spectra were recorded on a LCQ DECA XP quadrupole ion trap mass spectrometer and mass spectra of ligands **L1**–**L4** and complexes **1·BF$_4$**–**4·BF$_4$**, **1·PF$_6$**, **1·ClO$_4$** and **4·F** are listed in Fig. S37 and S38 (ESI†), respectively. Elemental analysis was performed on an Elemental Vario EL elemental analyzer.

Crystal structure determination

Crystals were grown by diffusion of diethyl ether into concentrated solution of the corresponding complexes. Single crystals of **1·BF$_4$**–**4·BF$_4$**, **1·PF$_6$**, **1·ClO$_4$** and **4·F** were carefully picked and coated in paratone oil, attached to a glass silk inserted in a stainless steel stick, then quickly transferred to the Agilent Gemini S Ultra CCD Diffractometer with the Enhance X-ray Source of Cu radiation (λ = 1.54178 Å) using the ω-ϕ scan technique. Structural solution and refinement against F^2 were carried out using the SHELXL programs.[70] Hydrogen atoms were placed in geometrically calculated positions and included in the refinement process using riding model with isotropic thermal parameters: U_{iso}(H) = 1.2U_{eq}(-CH). For structures of **1·BF$_4$**–**4·BF$_4$**, **1·ClO$_4$** and **4·F**, the contribution of heavily disordered solvent molecules was treated by the Squeeze procedure implemented in Platon.[71–72] Crystallographic data for the structures reported in this paper have been deposited in the Cambridge Crystallographic Data Centre as supplementary publication, CCDC 1421592–1421598 for **1·BF$_4$**, **1·ClO$_4$**, **1·PF$_6$**, **2·BF$_4$**–**4·BF$_4$** and **4·F**.

Titrations

For a typical ^{1}H NMR titration experiment, 1 μL aliquots of a tetra-*n*-butylammonium salt (5.00×10^{-1} mol·dm^{-3} in DMSO–d_6) were added into the 0.5 mL solution of the copper(I) acetylide complex in DMSO–d_6 (5.00×10^{-3} mol·dm^{-3}) by a syringe, and the ^{1}H NMR spectral changes were recorded by a Varian Mercury–Plus 300 spectrometer at 298 K.

Synthesis

General procedure for the synthesis of H-C≡CC$_6$H$_4$-4-NHC(O)-C$_6$H$_4$-R (R = NO$_2$ (L1), CF$_3$ (L2), H (L3), OCH$_3$ (L4)). To a solution of 4-ethylnylaniline and 1 equiv of the corresponding acyl chloride in $CHCl_3$ was added triethylamine. The mixture was heated to reflux for 18 h. The solvent was removed under reduced pressure, and the residue was washed with water and *n*-hexane to yield pale yellow solid.

L1. Yield: 123.5 mg, 56 %. ^{1}H NMR (DMSO–d_6, 298K): δ = 10.71 (s, 1H, NH), 8.36 (d, 2H, J = 9 Hz, aromatic ring), 8.16 (d, 2H, J = 9 Hz, aromatic ring), 7.80 (d, 2H, J = 9 Hz, aromatic ring), 7.48 (d, 2H, J = 9 Hz, aromatic ring), 4.15 (s, 1H, HC≡C). IR (KBr, cm^{-1}): ν = 3255 (N–H), 2098 (C≡C), 1654 (C=O). ESI-MS: m/z = 265 [M – H]$^-$. Anal. Calcd for $C_{15}H_{10}N_2O_3$ (%): C, 67.67; H, 3.79; N, 10.52. Found: C, 67.41; H, 3.80; N, 10.48.

L2. Yield: 139.8 mg, 60 %. ^{1}H NMR (DMSO–d_6, 298K): δ = 10.60 (s, 1H, NH), 8.12 (d, 2H, J = 9 Hz, aromatic ring), 7.91 (d, 2H, J = 8 Hz, aromatic ring), 7.80 (d, 2H, J = 9 Hz, aromatic ring), 7.47 (d, 2H, J = 9 Hz, aromatic ring), 4.14 (s, 1H, HC≡C). IR (KBr, cm^{-1}): ν = 3302 (N–H), 2116 (C≡C), 1657 (C=O). ESI-MS: m/z = 288 [M – H]$^-$. Anal. Calcd for $C_{16}H_{10}F_3NO$ (%): C, 66.44; H, 3.48; N, 4.84. Found: C, 66.40; H, 3.47; N, 4.83.

L3. Yield: 115.2 mg, 56 %. ^{1}H NMR (DMSO–d_6, 298K): δ = 10.40 (s, 1H, NH), 7.92 (d, 2H, J = 8 Hz, aromatic ring), 7.80 (d, 2H, J = 9 Hz, aromatic ring), 7.61–7.44 (m, 5H, aromatic ring), 4.12 (s, 1H, HC≡C). IR (KBr, cm^{-1}): ν = 3299 (N–H), 2106 (C≡C), 1659 (C=O). ESI-MS: m/z = 256 [M – H]$^-$. Anal. Calcd for $C_{15}H_{11}NO$ (%): C, 81.43; H, 5.01; N, 6.33. Found: C, 80.41; H, 5.01; N, 6.35.

L4. Yield: 174.2 mg, 59 %. ^{1}H NMR (DMSO–d_6, 298K): δ = 10.22 (s, 1H, NH), 7.93 (d, 2H, J = 9 Hz, aromatic ring), 7.79 (d, 2H, J = 8 Hz, aromatic ring), 7.43 (d, 2H, J = 9 Hz, aromatic ring), 7.05 (d, 2H, J = 9 Hz, aromatic ring), 4.10 (s, 1H, HC≡C), 3.83 (s, 3H, OCH_3). IR (KBr, cm^{-1}): ν = 3283 (N–H), 2106 (C≡C), 1658 (C=O). ESI-MS: m/z = 250 [M – H]$^-$. Anal. Calcd for $C_{16}H_{13}NO_2$ (%): C, 76.48; H, 5.21; N, 5.57. Found: C, 76.50; H, 5.22; N, 5.55.

[Cu$_3$(μ-dppm)$_3$(μ_3-η^1-C≡CC$_6$H$_4$-4-NHC(O)C$_6$H$_4$-4-NO$_2$)$_2$BF$_4$]$_\infty$ (1·BF$_4$). To a solution of $[Cu_2(\mu\text{-dppm})_2(CH_3CN)_4](BF_4)_2$ (100.8 mg, 0.082 mmol) and **L1** (29.0 mg, 0.11 mmol) in degassed CH_3CN (50 mL), NEt_3 (1 mL) was added. The mixture was stirred overnight under nitrogen. After evaporation to dryness, the solid residue was collected and washed with water and diethyl ether. Subsequent diffusion of diethyl ether into the concentrated CH_3CN solution gave orange crystals. Yield: 90.6 mg, 85 %.^{1}H NMR (CD_3CN, 298K): δ = 9.19 (s, 2H, NH), 8.40 (d, 4H, J = 9 Hz, aromatic ring), 8.21 (d, 4H, J = 9 Hz, aromatic ring), 7.90 (d, 4H, J = 9 Hz, aromatic ring), 7.47 (d, 4H, J = 9 Hz, aromatic ring), 7.18–6.83 (m, 60H, aromatic ring), 3.37 (s, 6H, CH_2). ^{31}P NMR (CD_3CN, 298K): δ = –5.96 (s). ^{19}F NMR (CD_3CN, 298K): δ = –151.65 (s, $^{10}BF_4^-$), –151.70 (s, $^{11}BF_4^-$). IR (KBr, cm^{-1}): ν = 3373 (N–H), 2138 (C≡C), 1672 (C=O). ESI-MS: m/z = 1874 [M]$^+$. Anal. Calcd for $C_{105}H_{84}Cu_3BF_4N_4O_6P_6$ (%): C, 64.31; H, 4.32; N, 2.86. Found: C, 64.34; H, 4.30; N, 2.87.

[Cu$_3$(μ-dppm)$_3$(μ_3-η^1-C≡CC$_6$H$_4$-4-NHC(O)C$_6$H$_4$-4-NO$_2$)$_2$PF$_6$]$_\infty$ (1·PF$_6$). To a solution of $[Cu_2(\mu\text{-dppm})_2(CH_3CN)_4](PF_6)_2$ (159.0 mg, 0.11 mmol) and **L1** (41.9 mg, 0.16 mmol) in degassed CH_3CN (50 mL), NEt_3 (1.5 mL) was added. The mixture was stirred overnight under nitrogen. After evaporation to dryness, the solid residue was collected and washed with water and diethyl ether. Subsequent diffusion of diethyl ether into the concentrated CH_2Cl_2 solution gave orange crystals. Yield: 147.6 mg, 93 %. ^{1}H NMR (CD_3CN, 298K): δ = 9.30 (s, 2H, NH), 8.54 (d, 4H, J = 9 Hz, aromatic ring), 8.34 (d, 4H, J = 9 Hz, aromatic ring), 8.04 (d, 4H, J = 9 Hz, aromatic ring), 7.61 (d, 4H, J = 9 Hz, aromatic ring), 7.32–6.97 (m, 60H, aromatic ring), 3.37 (s, 6H, CH_2). ^{31}P NMR (CD_3CN, 298K): δ = –5.95, –144.65 (quint, PF_6^-). ^{19}F NMR (CD_3CN, 298K): δ = –73.53 (d, J = 700 Hz). IR (KBr, cm^{-1}): ν = 3399 (N–H), 2321 (C≡C), 1677 (C=O). ESI-MS: m/z = 1874 [M]$^+$. Anal. Calcd for $C_{105}H_{84}Cu_3F_6N_4O_6P_7$ (%): C, 62.46; H, 4.19; N, 2.77. Found: C, 62.44; H, 4.15; N, 2.72.

[Cu$_3$(μ-dppm)$_3$(μ_3-η^1-C≡CC$_6$H$_4$-4-NHC(O)C$_6$H$_4$-4-NO$_2$)$_2$ClO$_4$]$_\infty$

(1·ClO$_4$). To a solution of [Cu$_2$(μ-dppm)$_2$(CH$_3$CN)$_4$](ClO$_4$)$_2$ (106.7 mg, 0.085 mmol) and **L1** (30.3 mg, 0.11 mmol) in degassed CH$_3$CN (50 mL), NEt$_3$ (1 mL) was added. The mixture was stirred overnight under nitrogen. After evaporation to dryness, the solid residue was collected and washed with water and diethyl ether. Subsequent diffusion of diethyl ether into the concentrated CH$_2$Cl$_2$ solution gave orange crystals. Yield: 98.0 mg , 88 %.^{1}H NMR (CD$_3$CN, 298K): δ = 8.98 (s, 2H, NH), 8.21 (d, 4H, J = 9 Hz, aromatic ring), 8.02 (d, 4H, J = 9 Hz, aromatic ring), 7.71 (d, 4H, J = 8 Hz, aromatic ring), 7.28 (d, 4H, J = 9 Hz, aromatic ring), 6.97–6.64 (m, 60H, aromatic ring), 3.04 (s, 6H, CH$_2$). ^{31}P NMR (CD$_3$CN, 298K): δ = –5.95 (s). IR (KBr, cm^{-1}): ν = 3387 (N–H), 2238 (C≡C), 1674 (C=O). ESI-MS: m/z = 1874 [M]$^+$. Anal. Calcd for C$_{105}$H$_{84}$Cu$_3$ClN$_4$O$_{10}$P$_6$ (%): C, 63.90; H, 4.29; N, 2.84. Found: C, 63.86; H, 4.27; N, 2.86.

[Cu$_3$(μ-dppm)$_3$(μ_3-η^1-C≡CC$_6$H$_4$-4-NHC(O)C$_6$H$_4$-4-CF$_3$)(μ_3-η^1-C≡CC$_6$H$_4$-4-NHC(O)C$_6$H$_4$-4-CF$_3$)BF$_4$]$_\infty$ (2·BF$_4$). To a solution of [Cu$_2$(μ-dppm)$_2$(CH$_3$CN)$_4$](BF$_4$)$_2$ (215.1 mg, 0.17 mmol) and **L2** (67.3 mg, 0.23 mmol) in degassed CH$_3$CN (50 mL), NEt$_3$ (1 mL) was added. The mixture was stirred overnight under nitrogen. After evaporation to dryness, the solid residue was collected and washed with water and diethyl ether. Subsequent diffusion of diethyl ether into the concentrated CH$_3$CN solution gave colorless crystals. Yield: 148.4 mg, 64 %. ^{1}H NMR (CD$_3$CN, 298K): δ = 9.09 (s, 2H, NH), 8.19 (d, 4H, J = 9 Hz, aromatic ring), 7.91 (d, 4H, J = 9 Hz, aromatic ring), 7.48 (d, 4H, J = 9 Hz, aromatic ring), 7.19–6.84 (m, 64H, aromatic ring), 3.23 (s, 6H, CH$_2$). ^{31}P NMR (CD$_3$CN, 298K): δ = –5.94 (s). ^{19}F NMR (CD$_3$CN, 298K): δ = –64.06 (s, CF$_3$), –151.71 (s, ^{10}BF$_4^-$), –151.77 (s, ^{11}BF$_4^-$). IR (KBr, cm^{-1}): ν = 3368 (N–H), 2262 (C≡C), 1674 (C=O). ESI-MS: m/z = 1920 [M]$^+$. Anal. Calcd for C$_{107}$H$_{84}$Cu$_3$BF$_6$N$_2$O$_2$P$_6$ (%): C, 66.92; H, 4.41; N, 1.46. Found: C, 66.82; H, 4.45; N, 1.46.

[Cu$_3$(μ-dppm)$_3$(μ_3-η^1-C≡CC$_6$H$_4$-4-NHC(O)C$_6$H$_5$)$_2$BF$_4$]$_\infty$ (3·BF$_4$). To a solution of [Cu$_2$(μ-dppm)$_2$(CH$_3$CN)$_4$](BF$_4$)$_2$ (72.4mg, 0.059 mmol) and **L3** (17.3 mg, 0.078 mmol) in degassed CH$_3$CN (50 mL), NEt$_3$ (1 mL) was added. The mixture was stirred overnight under nitrogen. After evaporation to dryness, the solid residue was collected and washed with water and diethyl ether. Subsequent diffusion of diethyl ether into the concentrated CH$_3$OH solution gave colorless crystals. Yield: 50.9 mg, 70 %. ^{1}H NMR (CD$_3$CN, 298K): δ = 8.98 (s, 2H, NH), 8.04 (d, 4H, J = 9 Hz, aromatic ring), 7.92 (d, 4H, J = 9 Hz, aromatic ring), 7.66–7.57 (m, 6H, aromatic ring), 7.48 (d, 4H, J = 9 Hz, aromatic ring), 7.19–6.86 (m, 60H, aromatic ring), 3.25 (s, 6H, CH$_2$). ^{31}P NMR (CD$_3$CN, 298K): δ = –5.98 (s). ^{19}F NMR (CD$_3$CN, 298K): δ = –151.67 (s, ^{10}BF$_4^-$), –151.72 (s, ^{11}BF$_4^-$). IR (KBr, cm^{-1}): ν = 3369 (N–H), 2238 (C≡C), 1656 (C=O). ESI-MS: m/z = 1784 [M]$^+$. Anal. Calcd for C$_{107}$H$_{84}$Cu$_3$BF$_6$N$_2$O$_2$P$_6$ (%): C, 66.92; H, 4.41; N, 1.46. Found: C, 66.93; H, 4.43; N, 1.43.

[Cu$_3$(μ-dppm)$_3$(μ_3-η^1-C≡CC$_6$H$_4$-4-NHC(O)C$_6$H$_4$-4-OCH$_3$)$_2$]BF$_4$ (4·BF$_4$). To a solution of [Cu$_2$(μ-dppm)$_2$(CH$_3$CN)$_4$](BF$_4$)$_2$ (114.8 mg, 0.093 mmol) and **L4** (31.6 mg, 0.13 mmol) in degassed CH$_3$CN (50 mL), NEt$_3$ (1.5 mL) was added. The mixture was stirred overnight under nitrogen. After evaporation to dryness, the solid residue was collected and washed with water and diethyl ether. Subsequent diffusion of diethyl ether into the concentrated acetone and methanol mixed solution gave yellow crystals. Yield: 73.9 mg, 62 %.^{1}H NMR (CD$_3$CN, 298K): δ = 8.90 (s, 2H, NH), 8.04 (d, 4H, J = 9 Hz, aromatic ring), 7.92 (d, 4H, J = 9 Hz, aromatic ring), 7.48 (d, 4H, J = 9 Hz, aromatic ring), 7.18–6.85 (m, 64H, aromatic ring), 3.94 (s, 6H, CH$_3$), 3.24 (s, 6H, CH$_2$). ^{31}P NMR (CD$_3$CN, 298K): δ = –6.04 (s). ^{19}F NMR (CD$_3$CN, 298K): δ = –151.65 (s, ^{10}BF$_4^-$), –151.70(s, ^{11}BF$_4^-$). IR (KBr, cm^{-1}): ν = 3371 (N–H), 2246 (C≡C), 1662 (C=O). ESI-MS: m/z = 1844 [M]$^+$. Anal. Calcd for C$_{107}$H$_{90}$Cu$_3$BF$_4$N$_2$O$_4$P$_6$ (%): C, 66.55; H, 4.70; N, 1.45. Found: C, 66.52; H, 4.71; N, 1.46.

[Cu$_3$(μ-dppm)$_3$(μ_3-η^1-C≡CC$_6$H$_4$-4-NHC(O)C$_6$H$_4$-4-OCH$_3$)$_2$F]$_\infty$ (4·F). To a solution of **4·BF$_4$** (76.8 mg, 0.062 mmol) in CH$_3$CN, NBu$_4$F (102.3 mg, 0.39 mmol) in CH$_3$CN was added dropwise. The mixture was stirred overnight. The yellow precipitate was collected and washed by acetonitrile. Subsequent diffusion of diethyl ether into the concentrated CH$_3$OH solution gave pale yellow crystals. Yield: 9.0 mg, 12 %. ^{1}H NMR (DMSO–d_6, 298K): δ = 8.12 (d, 4H, J = 9 Hz, aromatic ring), 7.92 (d, 4H, J = 9 Hz, aromatic ring), 7.26 (d, 4H, J = 9 Hz, aromatic ring), 7.20–6.83 (m, 64H, aromatic ring), 3.87 (s, 6H, CH$_3$), 3.15 (s, 6H, CH$_2$). ^{31}P NMR (DMSO–d_6, 298K): δ = –6.04 (s). IR (KBr, cm^{-1}): ν = 3429 (N–H), 2291 (C≡C), 1654 (C=O). ESI-MS: m/z = 1844 [M]$^+$. Anal. Calcd for C$_{107}$H$_{90}$Cu$_3$FN$_2$O$_4$P$_6$ (%): C, 68.97; H, 4.87; N, 1.50. Found: C, 68.90; H, 4.85; N, 1.51.

Acknowledgements

We acknowledge financial support from the National Natural Science Foundation of China (20971131 and J1103305), the Natural Science Foundation of Guangdong Province (S2012010010566), and the Undergraduate Innovative Experiment Program of Sun Yat-sen University (201504020055). We thank Dr. Xiao-Long Feng for crystallographic data collection.

Notes and references

MOE Key Laboratory of Bioinorganic and Synthetic Chemistry, School of Chemistry and Chemical Engineering, Sun Yat-sen University, Guangzhou 510275, P. R. China. E-mail: zhaoxy@mail.sysu.edu.cn; Fax: +86-20-84112245; Tel: +86-20-84110062.

Electronic Supplementary Information (ESI) available: X-ray crystallographic files in CIF format for complexes **1·BF$_4$–4·BF$_4$**, **1·PF$_6$** **1·ClO$_4$** and **4·F**. Additional figures and tables. See DOI: 10.1039/b000000x/.

1. N. Busschaert, C. Caltagirone, W. V. Rossom and P. A. Gale, *Chem. Rev.*, 2015, **115**, 8038 –8155.
2. F. Wang, L. Wang, X. Chen and J. Yoon, *J. Chem. Soc. Rev.*, 2014, **43** 4312–4324
3. P. A. Gale, N. Busschaert, C. J. E. Haynes, L. E. Karagiannidis and I. L. Kirby, *Chem. Soc. Rev.*, 2014, **43**, 205–241.
4. L. Fabbrizzi and A. Poggi, *Chem. Soc. Rev.*, 2013, **42**, 1681–1699.
5. K. Bowman-James, A. Bianchi and E. García-Espana, *Anion Coordination Chemistry*, Wiley, New York, 2012.
6. P. A. Gale, *Acc. Chem. Res.*, 2011, **44**, 216–226.
7. V. Amendola, D. Esteban-Gómez, L. Fabbrizzi and M. Licchelli, *Acc. Chem. Res.*, 2006, **39**, 343–353.
8. K. Bowman-James, *Acc. Chem. Res.*, 2005, **38**, 671–678.
9. C. H. Park and H. E. Simmons, *J. Am. Chem. Soc.*, 1968, **90** 2431–2432.
10. J. M. Lehn, *Acc. Chem. Res.*, 1978, **11**, 49–57.
11. P. D. Beer and P. A. Gale, *Angew. Chem. Int. Ed.*, 2001, **40**, 486–516.
12. M. R. Sambrook, P. D. Beer, J. A. Wisner, R. L. Paul, A. R. Cowley, F. Szemes and M. G. B. Drew, *J. Am. Chem. Soc.*, 2005, **127**, 2292–2302.
13. M. R. Sambrook, P. D. Beer, J. A. Wisner, R. L. Paul and A. R. Cowley, *J. Am. Chem. Soc.*, 2004, **126**, 15364–15365.
14. James A. Wisner, Paul D. Beer, Neil G. Berry and B. Tomapatanaget, *Proc. Natl. Acad. Sci.*, 2002, **99**, 4983–4986.
15. J. A. Wisner, P. D. Beer, M. G. B. Drew and M. R. Sambrook, *J. Am. Chem. Soc.*, 2002, **124**, 12469–12476.
16. G. W. Bates, P. A. Gale and M. E. Light, *Chem. Commun.*, 2007, **21**,

2121–2123.
17. S. J. Brooks, P. A. Gale and M. E. Light, *CrystEngComm*, 2005, **7**, 586–591.
18. C. R. Bondy, P. A. Gale and S. J. Loeb, *J. Am. Chem. Soc*., 2004, **126**, 5030–5031.
19. S. J. Coles, J. G. Frey, P. A. Gale, M. B. Hursthouse, M. E. Light, K. Navakhun and G. L. Thomas, *Chem. Commun*., 2003, **5**, 568–569.
20. P. Byrne, G. O. Lloyd, K. M. Anderson, N. Clarke and J. W. Steed, *Chem. Commun.*, 2008, **32**, 3720–3722.
21. J. M. Russell, A. D. M. Parker, I. Radosavljevic-Evans, J. A. K. Howard and J. W. Steed, *CrystEngComm*, 2006, **8**, 119–122.
22. C. A. llioudis, D. A. Tocher and J. W. Steed, *J. Am. Chem. Soc.*, 2004, **126**, 12395–12402.
23. K. J. Wallace, W. J. Belcher, D. R. Turner, K. F. Syed and J. W. Steed, *J. Am. Chem. Soc.*, 2003, **125**, 9699–9715.
24. R. Custelcean, P. V. Bonnesen, N. C. Duncan, X. H. Zhang, L. A. Watson, G. Van Berkel, W. B. Parson and B. P. Hay, *J. Am. Chem. Soc.*, 2012, **134**, 8525–8529.
25. R. Custelcean, A. Bock and B. A. Moyer, *J. Am. Chem. Soc.*, 2010, **132**, 7177–7185.
26. R. Custelcean, J. Bosano, P. V. Bonnesen, V. Kertesz and B. P. Hay, *Angew. Chem., Int. Ed.*, 2009, **48**, 4025–4020.
27. R. Custelcean, P. Remy, P. V. Bonnesen, D. E. Jiang and B. A. Moyer, *Angew. Chem. Int. Ed.*, 2008, **47**, 1866–1870.
28. J. Wang, S. Li, P. Yang, X. Huang, X. J. Yang and B. Wu, *CrystEngComm*, 2013, **15**, 4540–4548.
29. S. G. Li, M. Y. Wei, X. J. Huang, X. J. Yang and B. Wu, *Chem. Commun.*, 2012, **48**, 3097–3099.
30. S. G. Li, C. D. Jia, B. Wu, Q. Luo, X. J. Huang, Z. W. Yang, Q. S. Li and X. J. Yang, *Angew. Chem. Int. Ed.*, 2011, **50**, 5721–5724.
31. C. D. Jia, B. A. Wu, S. G. Li, X. J. Huang, Q. L. Zhao, Q. S. Li and X. J. Yang, *Angew. Chem. Int. Ed.*, 2011, **50**, 486–490.
32. Z. W. Yang, B. Wu, X. J. Huang, Y. Y. Liu, S. G. Li, Y. N. Xia, C. D. Jia and X. J. Yang, *Chem. Commun.*, 2011, **47**, 2880–2882.
33. M. Wenzel, J.R. Hiscock and P.A. Gale, *Chem. Soc. Rev.*, 2012, **41**, 480–520.
34. V. Amendola, L. Fabbrizzi and L. Mosca. *Chem. Soc. Rev.*, 2010, **39**, 3889–3915.
35. R. Vilar, *Eur. J. Inorg. Chem.*, 2008, **3**, 357–367.
36. P. A. Gale, *Acc. Chem. Res.*, 2006, **39**, 465–475.
37. H. Maeda and Y. Kusunose, *Chem. Eur. J.*, 2005, **11**, 5661–5666.
38. W. L. Leong and J. J. Vittal, *Chem. Rev.*, 2011, **111**, 688–764.
39. S. Kitagawa, R. Kitaura and S. Noro, *Angew. Chem. Int. Ed.*, 2004, **43**, 2334–2375.
40. H. Juwarker and K. S. Jeong. *Chem. Soc. Rev.*, 2010, **39**, 3664–3674.
41. J. Sánchez-Quesada, C. Seel, P. Prados and J. de Mendoza, *J. Am. Chem. Soc.*, 1996, **118**, 277–278.
42. J. W. Steed, *Chem. Soc. Rev.*, 2009, **38**, 506–519.
43. S. K. L. Siu, C. C. Ko, V. K. M. Au and V. W. W. Yam, *J. Clust. Sci.*, 2014, **25**, 287–300.
44. V. W. W. Yam, K. K. W. Lo and K. M. C. Wong, *J. Organomet. Chem.*, 1999, **578**, 3–30.
45. V. W. W. Yam, K. K. W. Lo, W. K. M. Fung and C. R. Wang, *Coord. Chem. Rev.*, 1998, **171**, 17–41.
46. V. W. W. Yam, W. K. M. Fung and K. K. Cheung, *Angew. Chem. Int. Ed.*, 1996, **35**, 1100–1102.
47. V. W. W. Yam, W. K. Lee and T. F. Lai, *Organometallics*, 1993, **12**, 2383–2387.
48. J. Diéz, M.P. Gamasa, J. Gimeno, A. Aguirre and S. García-Granda, *Organometallics*, 1991, **10**, 380–382.
49. M. Zhang, B. C. Su, C. L. Li, Y. Shen, C. K. Lam, X. L. Feng and H. Y. Chao, *J. Organomet. Chem.*, 2011, **696**, 2654–2659.
50. P. Dydio, D. Lichosyt and J. Jurczak, *Chem. Soc. Rev.*, 2011, **40**, 2971–2985.
51. D. Voet, J.G. Voet and C.W. Pratt, *Fundamentals of Biochemistry*, Wiley, New York, 1999.
52. C. Caltagirone and P. A. Gale, *Chem. Soc. Rev.*, 2009, **38**, 520–563.
53. D. W. Yoon, H. Hwang and C. H. Lee, *Angew. Chem. Int. Ed.*, 2002, **41**, 1757–1759.
54. K. Chellappan, N. J. Singh, I. C. Hwang, J. W. Lee and K. S. Kim, *Angew. Chem. Int. Ed.*, 2005, **44**, 2899–2903.
55. K. Sato, S. Arai and T. Yamagishi, *Tetrahedron Lett.*, 1999, **40**, 5219–5222.
56. H. Ihm, S. Yun, H. G. Kim, J. K. Kim and K. S. Kim, *Org. Lett.*, 2002, **4**, 2897–2900.
57. R. Vargas, J. Garza, D. A. Dixon and B. P. Hay, *J. Am. Chem. Soc.*, 2000, **122**, 4750–4755.
58. V. S. Bryantsev and B. P. Hay, *J. Am. Chem. Soc.*, 2005, **127**, 8282–8283.
59. H. Y. Shi, J. Qi, Z. Z. Zhao, W. J. Feng, Y. H. Li, L. Sun, Z. J. Lin and H. Y. Chao, *New J. Chem*., 2014, **38**, 6168–6175.
60. J. C. Slater, *J. Chem. Phys*., 1964, **41**, 3199–3204.
61. R. Nast, *Coord. Chem. Rev*., 1982, **47**, 89–124.
62. D. Esteban-Gomez, L. Fabbrizzi and M. Liechelli, *J. Org. Chem*., 2005, **70**, 5717–5720.
63. M. Boiocchi, L. DelBoca, D. Esteban-Gomez, L. Fabbrizzi, M. Licchelli and E. Monzani, *Chem. Eur. J*., 2005, **11**, 3097–3104.
64. M. Boiocchi, L. DelBoca, D. E. Gomez, L. Fabbrizzi, M. Licchelli and E. Monzani, *J. Am. Chem. Soc*., 2004, **126**, 16507–16514.
65. X. He, F. Herranz, E. C. Cheng, R. Vilar and V. W. W. Yam, *Chem. Eur. J.*, 2010, **16**, 9123–9131.
66. A. B. Descalzo, K. Rurack, H. Weisshoff, R. Martínez-Máñez, M. D. Marcos, P. Amorós, K. Hoffmann and J. Soto, *J. Am. Chem. Soc.*, 2005, **127**, 184–200.
67. C. Jia, B. Wu, J. Liang, X. Huang and X. Yang, *J. Fluoresc.*, 2010, **20**, 291–297.
68. J. Diéz, M.P. Gamasa, J. Gimeno, A. Tiripicchio and M.T. Gamellini, *J. Chem. Soc. Dalton Trans*., 1987, 1275–1278.
69. J. N. Demas and G. A. Crosby, *J. Phys. Chem*., 1971, **75**, 991–1024.
70. G. M. Sheldrick, *SHELX 97, Program for Crystal Structure Solution and Refinement*, *Göttingen University*, 1997.
71. V. A. Blatova, *IUCr Comp. Comm. Newslett., 2*006, **7**, 4–38.
72. V. A. Blatova and D. M. Proserpio, *ActaCrystallogr A,* 2009, **65**, 202–212.